Controlling submicron particle deposition in a side-stream membrane bioreactor: A theoretical hydrodynamic modelling approach incorporating energy consumption

Tao Jiang [a,b,*], Maria D. Kennedy [b], ChangKyoo Yoo [c], Ingmar Nopens [a], Walter van der Meer [d], Harry Futselaar [e], Jan C. Schippers [b], Peter A. Vanrolleghem [a,f]

[a] *BIOMATH, Ghent University, Coupure Links 653, B-9000 Gent, Belgium*
[b] *UNESCO-IHE for Water Education, P.O. Box 3015, 2601 DA Delft, the Netherlands*
[c] *College of Environmental and Applied Chemistry/Center for Environmental Studies, Kyung Hee University, Yongin-city, Gyeonggi-do 446-701, South Korea*
[d] *Vitens Fryslân, Snekertrekweg 61, Postbus 400, 8901 BE Leeuwarden, the Netherlands*
[e] *Norit Process Technology B.V., P.O. Box 741, 7500 AS ENSCHEDE, the Netherlands*
[f] *modelEAU, Département de génie civil, Pavillon Pouliot, Université Laval, Québec, QC, G1K 7P4, Canada*

Abstract

Soluble microbial products (SMP) in the sludge water phase are regarded as the main foulant in MBRs. This study further developed an existing hydrodynamic model by incorporating energy consumption. The focus was on the cost-effectiveness of crossflow (CF) velocity in the control of submicron particle deposition. A sensitivity analysis showed that CF had the greatest impact on both particle backtransport and energy consumption. The other operational variables, i.e., dry solid content (DS), membrane tube dimension (D and L) and temperature (T) were generally less influential with respect to particle backtransport and energy consumption. Submicron particles were likely to deposit in side-stream MBRs, and the lowest backtransport velocity was found for particle radii around 0.1 μm and CF below 0.5 m/s. A particle size distribution (PSD) profile of MBR sludge showed a main peak at 40 μm and a second peak at 0.1–1 μm. The abundance of submicron particles at 2000 kDa was confirmed by a Liquid chromatography–Organic Carbon Detection (LC-OCD) analysis. The colloids responsible for the second peak in the PSD received high weighting factors (high filter cake formation potential) in the model optimization. In a lab-scale MBR, this critical crossflow velocity was between 0.75 and 1 m/s at 40 L/(m² h).
© 2007 Elsevier B.V. All rights reserved.

Keywords: Membrane bioreactor; Fouling; Hydrodynamics; Modelling; Optimization

1. Introduction

Membrane bioreactors (MBRs) are an innovative activated sludge process using membrane filtration instead of secondary clarifiers to achieve biomass separation. The microfiltration or ultrafiltration membrane produces excellent effluent quality free of particulates and coliforms, which is suitable for many reuse applications [1]. The high sludge concentration and the elimination of secondary clarifiers save space, which makes the MBR an attractive option for space limited situations (e.g., upgrading of existing wastewater treatment plants). Recently, rapidly decreasing membrane costs is another important driving force for the widespread application of MBRs [1]. However, membrane fouling and high energy consumption remain the main drawbacks. It is generally accepted that biology, membrane characteristics, configuration, and operational conditions of membrane modules all play important roles in membrane fouling control.

The composition of activated sludge in MBRs is very complex, and includes natural organic matter (hundreds to thousands

Da) introduced from potable water, SMPs (soluble microbial products or called soluble EPS) produced by the biomass (a few thousand Da to a few million Da), viruses and single bacterial cells (a few dozen nm to a few μm) and protozoa and flocs (a few μm to a few hundred μm), etc. Some early studies on the relative contribution of each sludge fraction (solutes, colloids and particulates) to membrane fouling appear contradictive, Wisniewski and Grasmick reported 52%, 25% and 23% [2]; Defrance et al. reported 5%, 30% and 65% [3]; and Bouhabila et al. reported 25%, 50% and 24%, respectively [4]. However, more recent studies reveal that the SMPs in the sludge water phase are closely correlated with MBR fouling. Rojas et al. reported that the change in the filtration resistance was positively correlated with the COD in the sludge supernatant, and specifically the protein concentration [5]. Lesjean et al. used size exclusion chromatography (SEC) to analyze the sludge water phase and concluded that the large organic molecules present in the sludge water phase (i.e., polysaccharides, proteins and organic colloids) impacted the MBR fouling [6,7]. Rosenberger et al. summarized 6 MBR case studies of different European research groups. The results showed a clear relevance of sludge liquid phase constitutes, either colloidal or soluble, with membrane fouling [8]. Poele et al. fractionated sludge water into a series of fractions according to their sizes and concluded that the colloidal particles in a range of 0.1–0.45 μm had the most significant contribution to the filterability of WWTP effluent [9].

In side-stream MBRs, crossflow filtration is employed to control particle deposition onto the membrane surface. The hydrodynamics of tubular membrane systems have been intensively studied in the 1980s and 1990s. An excellent review has been provided by Belfort et al. on particle backtransport mechanisms and models [10], including the concentration polarization (Brownian diffusion) model, the shear-induced diffusion model and the inertial lift model. Tardieu et al. applied these models to compare fouling rates at different crossflow velocities and filtration fluxes in a side-stream MBR equipped with tubular membranes [11]. The simulation showed that increasing crossflow velocity improved particle back transport and reduced membrane fouling. The simulation results were confirmed by experiments [11,12]. However, the study focussed on fouling resulting from large particles (above one micrometer), and less attention was paid to the colloidal particles and macromolecules. In addition, high crossflow velocities (2–4 m/s) and high TMPs (up to 2×10^5 Pa (2 bars)) were employed. However, the new generation of side-stream MBRs in operation today usually employ a suction pump on the permeate side of the membrane, allowing operating the membrane at low TMP (0.05–0.2×10^5 Pa (0.05–0.2 bar)) and low CF (0.5–1 m/s) to save energy [13,14]. For example, the new concept air-lift is applied with reduced energy consumption [15].

This study attempts to correlate the deposition of submicron particles with membrane fouling in the new generation of energy efficient side-stream MBRs. LC-OCD was employed to determine the particle size distribution of submicron particles [16]. The objectives of this study are (1) to further develop existing hydrodynamic models by incorporating energy consumption; (2) to quantify the cost-effectiveness of crossflow in the control of submicron particle deposition, and (3) to optimize the operational conditions of side-stream MBR systems using the improved model.

2. Theory

2.1. Flow in the membrane tube

The Reynolds number (Re) of the sludge circulating in a membrane tube can be estimated by $\rho_f U D / \eta_f$, where U is the crossflow velocity (m/s), D is the membrane tube diameter (m) and η_f is the feed sludge viscosity (Pa s) [17]. The specific density of feed activated sludge (ρ_f, kg/m^3) can be estimated by DS $+ 1000(1 - DS/\rho_{DS})$, where ρ_s (kg/m^3) is the specific density of dry solids, $\rho_{DS} = 1250$ kg/m^3 [18] and DS (g/L) is the dry solid contents of the activated sludge.

An activated sludge leads to typical non-Newtonian flow. The sludge viscosity decreases with increasing shear rate and approaches a constant, the "limit viscosity". Considering the high shear rate (typically >1000 s^{-1} calculated in the subsequent sections of this paper) in the membrane tube of side-stream MBRs, the "limit viscosity" often applies. The activated sludge viscosity can be expressed as a function of the dry solid contents, which can be determined by an exponential law, e.g., in Eq. (1) [19].

$$\eta_f = 9.968 \times 10^{-4} \cdot e^{0.0934 \cdot DS} \tag{1}$$

The temperature effect on viscosity can be estimated by Eq. (2) [17], where T_0 and T are the absolute temperature under the field and standard (293.15 K) conditions; η_{f0} and η_f are the corresponding viscosities; $a = -1.94$; $b = -4.80$ and $c = 6.74$. However, it should be noted that Eqs. (1) and (2) are empirical and not optimized for this study. The actual sludge viscosity may deviate from the values derived from them.

$$\ln \frac{\eta_f}{\eta_{f0}} \approx a + b \left(\frac{T_0}{T} \right) + c \left(\frac{T_0}{T} \right)^2 \tag{2}$$

2.2. Headloss, shear stress and shear rate in the membrane tube

The headloss of feed sludge passing through the membrane tube (h_f, m water column) can be estimated by $fLU^2/(2gD)$, where f is the Darcy friction factor determined by either Eq. (3) or Eq. (4), and L is the membrane tube length (m) [17].

$$f = \frac{64}{Re} \quad (Re < 2300) \tag{3}$$

$$f = 0.316 \times Re^{-1/4} \quad (Re > 2300) \tag{4}$$

The wall shear stress (τ_w, Pa) and shear rate (γ_w, s^{-1}) at the surface of the membrane can be estimated from Eq. (5) and (6), respectively [17].

$$\tau_w = \frac{f \rho_f U^2}{8} \tag{5}$$

$$\gamma_w = \frac{\tau_w}{\eta_f} \tag{6}$$

2.3. Energy consumption of the membrane module

Only energy consumption associated with the membrane (module) in the side-stream MBR is considered in this study. Energy consumption in the biological process (e.g., due to aeration) is beyond the scope of this study. Energy consumption due to the crossflow in the membrane tube and the suction pump (E_c and E_f, W) can be estimated using Eq. (7) and (8), respectively, where Q_f and Q_p are the volumetric flow rates through the membrane tube (m^3/s); ρ_p is the density of permeate (kg/m^3); and ΔP_f is the pressure difference during filtration (Pa).

$$E_c = Q_f \rho_f g h_f \tag{7}$$

$$E_f = Q_p \Delta P_f \tag{8}$$

The specific energy consumption to obtain a net unit volume of filtrate ($\hat{E}_c$, J/m^3) due to the crossflow can be estimated by Eq. (9), where J_f is the filtration flux (gross flux, m^3/(m^2 s)); J_{BW} is the backwashing flux (m^3/(m^2 s)); t_f and t_{BW} are the duration of one filtration and backwashing cycle (s); t_{tot} is the total cycle time (filtration + backwashing) (s); and A is the total membrane surface area (m^2).

$$\hat{E}_c = \frac{Q_f \rho_f g h_f t_{tot}}{\int_{t=0}^{t_f} J_f \cdot A \cdot dt - \int_{t=0}^{t_{BW}} J_{BW} \cdot A \cdot dt} \tag{9}$$

Similarly, the specific energy consumption to obtain a net unit volume of filtrate ($\hat{E}_f$, J/m^3) due to filtration (suction and backwashing) can be estimated using Eq. (10), where ΔP_{BW} is the pressure difference during backwashing (Pa).

$$\hat{E}_f = \frac{\int_{t=0}^{t_f} J_f \cdot A \cdot \Delta P_f \cdot dt + \int_{t=0}^{t_{BW}} J_{BW} \cdot A \cdot \Delta P_{BW} \cdot dt}{\int_{t=0}^{t_f} J_f \cdot A \cdot dt - \int_{t=0}^{t_{BW}} J_{BW} \cdot A \cdot dt} \tag{10}$$

The specific total energy consumption of the membrane module ($\hat{E}_{tot}$, J/m^3) can be easily obtained by the sum of $\hat{E}_c$ and $\hat{E}_f$. It should be noted that Eq. (9) and (10) are only valid when the full length of membrane tubes are used for filtration, and there are no membrane tubes plugged by sludge (see Section 5.1).

2.4. Particle backtransport velocity

When particles enter the membrane tube and come close to the membrane surface, two forces are imposed on particles, i.e., the convective force towards the membrane surface (due to the drag force of permeation flow) and the shear force (due to crossflow velocity). The particle backtransport mechanisms include concentration polarization (Brownian diffusion, influencing small colloids), shear-induced diffusion and inertial lift (influencing big particles [10,20]). Recent investigations reported that particle–particle and particle–membrane interactions (including entropy, van der Waals interactions and electrostatic interactions) may also play important roles in particle transportation to/from the membrane surface, especially in concentrated solutions of colloidal particles [20,21]. However, they are not considered in this study.

Brownian diffusion is a random movement resulting from the bombardment of particles by water molecules. The Brownian diffusion coefficient D_B (m^2/s) can be estimated from the Stokes–Einstein relationship (Eq. (11)) [20], where k is the Boltzmann constant (1.38×10^{-23} kg m^2/s^2), T is the absolute temperature (K) and a is the particle radius (m), assuming spherical particles.

$$D_B = \frac{kT}{6\pi\eta_f a} \tag{11}$$

Trettin and Doshi derived the particle backtransport velocity due to Brownian diffusion J_B (m/s) for a dilute solution under laminar flow conditions (Eq. (12), [10]), where Φ_b and Φ_w are the particle volume fractions in the bulk and at the edge of the cake layer, respectively. Combining Eq. (11) and (12) yields Eq. (13).

$$J_B = 1.31\left(\frac{\gamma_w D_B^2}{L}\frac{\Phi_w}{\Phi_b}\right)^{1/3} \tag{12}$$

$$J_B = 0.185\left(\frac{\gamma_w k^2 T^2}{\eta_f^2 a^2 L}\frac{\Phi_w}{\Phi_b}\right)^{1/3} \tag{13}$$

The Brownian diffusion model underestimates the particle backtransport, and the deviation is more pronounced for large particles and at high shear rate conditions [10]. A possible explanation for this phenomenon may be that some other backtransport mechanisms are not included in the model. To solve the problem, a possible mechanism, the shear-induced hydrodynamic diffusivity model, was introduced by Zydney and Colton [22]. Shear-induced diffusion occurs because individual particles undergo random displacements from the streamlines in a shear flow as they interact with and tumble over other particles. Davis and Sherwood further developed the shear-induced diffusion model, and the backtransport velocity due to shear-induced diffusion (J_s) for a dilute solution ($\Phi_b < 0.1$) is as follows [23]:

$$J_s = 0.072\gamma_w\left(\frac{a^4}{L}\frac{\Phi_w}{\Phi_b}\right)^{1/3} \tag{14}$$

In addition, an inertial lift mechanism was also proposed by Belfort and co-workers [24,25]. Inertial lift involves a lateral migration of particles, which transports particles away from the membrane. The backtransport velocity due to inertial lift (J_I) of spherical particles in a dilute suspension under fast laminar flow conditions (channel Reynolds numbers large compared to unity) can be estimated as follows [10]:

$$J_I = 0.036\frac{\rho_f a^3 \gamma_w^2}{\eta_f} \tag{15}$$

These three particle backtransport mechanisms work simultaneously, and the total backtransport velocity (J_{tot}) is assumed to be the sum of them. The contribution of the individual mechanisms to the total backtransport velocity mainly depends on particle size and crossflow velocity, etc., which will be illustrated in Section 5.1.

3. Experimental

A side-stream lab-scale MBR system for biological COD, nitrogen and phosphorus removal equipped with a tubular UF module was built for this study. A municipal-like synthetic wastewater [26] was treated with an influent flow rate of 108 L/day and a filtration flux of 31.8 L/(m² h). The HRT (hydraulic retention time), total SRT (solid retention time) and aerobic SRT were controlled at 6.4 h, 17 days and 7.2 days, respectively. The PVDF membrane module (X-Flow, the Netherlands) had a total membrane surface area of 0.17 m², a normalized pore size of 0.03 μm, a membrane tube diameter of 5.2 mm and a length of 1 m. The only differences between this lab-scale module and a full-scale one are the tube length (3 m in a full-scale) and the number of tubes in a module (600 in full-scale). The membrane was backwashed for 18 s at 106 L/(m² h) and relaxed for 7 s every 7.5 min of filtration.

The sludge water phase was fractionated by centrifugation and subsequent filtration. Firstly, the sludge was centrifuged at $3000 \times g$ for 7 min to remove large flocs. The supernatant was first filtered through a glass microfibre filter (GF/C, 1.2 μm, Whatman, UK) and thereafter, the second filtration step was performed using a flat sheet microfiltration membrane (DURAPORE 0.45 μm PVDF, Millipore, USA) in a stirred cell (Stirred Cell 8200, Millipore, USA). The two step filtration avoided the build up of a thick filter cake. The final permeate is defined as the water phase of the sludge including colloids, macroorganic matters and solutes.

The sludge was filtered using a stirred cell unit (Stirred Cell 8200, Millipore, USA). However, the stirred cell unit was not stirred during operation in order to have dead-end filtration. A flat sheet 0.03 μm PVDF membrane was specially made for these batch filtration tests (X-flow, the Netherlands) with exactly the same material, structure and morphology as the tubular membrane employed in the lab and full-scale MBR systems. The feed was supplied by a constant head high level tank (TMP = 14.3 kPa, close to the practical TMP applied in full-scale MBRs).

The particle size distribution of MBR sludge flocs was measured using a MastersizerS (Malvern, UK). To obtain a better resolution in characterising the size of sub-micron particles, a new tool LC-OCD was applied (DOC-LABOR, Dr. Huber, Germany). The LC-OCD was equipped with a coarse size exclusion chromatography (SEC) column (Altech, Germany) filled with Toyopearl resin (HW-65S with pores size of 100 nm) and an organic carbon detector [16]. The SEC separates the sub-micron particles by their sizes and the organic carbon detector quantifies the amount of organic colloids.

4. Simulation and sensitivity analysis

A tubular UF membrane module used in full-scale MBRs (F4385 membrane, 38PRV module, X-Flow, the Netherlands) was used as a reference tubular membrane in the model simulation. This UF membrane (average pore size = 0.03 μm) module comprises 600 membrane tubes. Each membrane tube is 3 m long and the inner diameter is 5.2 mm. The other operational

Table 1
Fixed operational variables or parameters in the simulation

Parameter/variable	Reference values
Φ_w/Φ_b	60
Filtration flux	30 L/(m² h)
BW flux	6 × 30 L/(m² h)
Filtration TMP	0.1 × 10⁵ Pa (0.1 bar)
BW TMP	0.6 × 10⁵ Pa (0.6 bar)
Filtration/BW mode	300 s filtration/8 s BW

parameters and variables of the simulation are summarized in Tables 1 and 2.

In Table 1, the concentration polarization factor Φ_w/Φ_b is difficult to measure and it is assumed to be 60. At the critical condition of filter cake formation, the Φ_w equals the cake packing density (Φ_c). If one assumes $\Phi_w = \Phi_c = 0.6$ and $\Phi_b = 0.01$ (DS = 10 g/L), $\Phi_w/\Phi_b = 60$ will be obtained. However, it should be noted that: (1) the Φ_w/Φ_b ratio can vary depending on the extent of concentration polarization and bulk sludge DS; and (2) the Φ_w/Φ_b ratio is not a sensitive parameter, due to the fact that the backtransport velocity increases with the Φ_w/Φ_b ratio to a power of just 1/3 as in Eq. (12)–(14)). A small error in Φ_w/Φ_b ratio will not significantly influence the simulation results according to the sensitivity analysis (result not shown).

The absolute sensitivity (AS) and relative sensitivity (RS) were evaluated using Eq. (16) and (17), where, y and Δy are the model output variables and their variation; x and Δx are the model input parameters/variables and their variations.

$$AS = \frac{\Delta y}{\Delta x} \tag{16}$$

$$RS = \frac{\Delta y/y}{\Delta x/x} \tag{17}$$

RS is more attractive than AS because the magnitude of RS associated with each parameter is comparable. RS eliminates the influence of unit and absolute values of different parameters by considering their relative changes only. The criteria to evaluate RS are listed below.

RS < 0.25, the parameter has no significant influence on a model output;
$0.25 \le RS < 1$, the parameter is influential on a certain model output;
$1 \le RS < 2$, the parameter is very influential on a certain model output;

Table 2
The reference value and range of simulation of operational variables

Variables	Reference value	Range of simulation
T (°C)	15	5–30
DS (g/L)	10	2–30
a (μm)	0.1	0.01–100
U (m/s)	1	0.2–4
D (mm)	5.2	2–10
L (m)	3	1–5

RS ≥ 2, the parameter is extremely influential on a certain model output.

5. Results

5.1. Impact of crossflow velocity and particle radius

The Reynolds number, headloss and specific energy consumption of the membrane module are summarized in Table 3. At crossflow velocities above 0.23 m/s, which cover almost all MBR operational conditions, the specific energy consumption due to crossflow ($\hat{E}_c$) is considerably higher than the energy consumption of filtration ($\hat{E}_f$). This can be predicted according to the equations of Re, f and h_f by combining Eq. (3), (4), (7) and the Reynolds number equation. The specific energy consumption due to crossflow ($\hat{E}_c$) increases with the crossflow velocity to the power of 2 and 2.75 under laminar ($U < 1.1$ m/s) and turbulent flow ($U > 1.1$ m/s) conditions, respectively. Theoretical calculation shows the specific total energy consumption ($\hat{E}_{tot}$) in this membrane module is 0.245 kWh/m³ ($U = 1$ m/s). However, if one assumes that the overall efficiency of the pumps and electrical motors is 50%, the actual specific energy consumption of the membrane module (not including the energy consumption in the biology stage, e.g., aeration) will be 0.49 kWh/m³. This value is higher than that of the specific energy consumption (0.2–0.35 kWh/m³, membrane module only [27]) in submerged MBRs. The high energy consumption is a drawback of sidestream MBR systems [14].

The headloss along the membrane tube increases significantly with increasing CF velocity, which can result in a considerable heterogeneous distribution of TMP due to the decrease in feed pressure from the inlet to outlet. The local fluxes at the outlet may be considerably lower than the inlet, which cannot simply be measured by the global observation, e.g., flux and TMP. The headloss is estimated as 0.16×10^5 Pa (0.16 bar) at the reference conditions. Consequently, the TMP at the outlet of the membrane tube is 0.16×10^5 Pa (0.16 bar) lower than the inlet. The heterogeneous distribution of TMP is another disadvantage of high CF in addition to the energy consumption. However, this problem can be counterbalanced by introducing air into the feed (air lift) in vertical membrane module systems, which reduces the gravity head inside the tube near the inlet (bottom) [15].

Fig. 1 illustrates the particle backtransport velocity as a function of the feed sludge crossflow velocity and particle radius. To compare it with the permeation velocity, the filtration flux
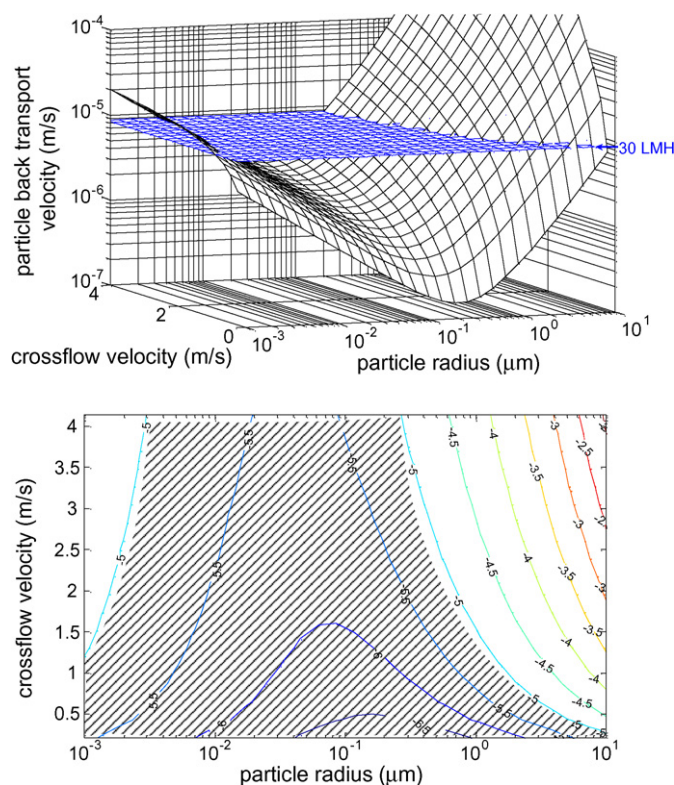

Fig. 1. The influence of crossflow velocity and particle size on the particle backtransport ($D = 5.2$ mm, $L = 3$ m, DS = 10 g/L, $T = 15$ °C, the numbers in the lower figure are the log 10 values of backtransport velocities).

is also plotted, i.e., 30 L/(m² h) (the equivalent log 10 value is −5.1 m/s). The shaded area in the lower figure is the region, in which the permeation velocity exceeds the backtransport velocity, and hence, in which case the particles have a higher likelihood to deposit. The critical particle size, on which the permeation and backtransport velocity are balanced, at $U = 1$ m/s is 1.5 μm. Increasing the CF up to 4 m/s is able to reduce the critical particle size down to 0.3 μm. On the other hand, for particles larger than 10 μm, even very low crossflow velocities (0.3 m/s) can keep them in suspension. Fortunately, the majority of MBR sludge particles are larger (in dimension) than 10 μm [3,28], although some studies reported small particle sizes (1–2 μm) [29].

The above theoretical simulation suggests that submicron particles have a high likelihood to deposit, and simply increasing CF may not completely prevent their deposition. The worst region is when the particle radii are around 0.1 μm and CF below

Table 3
The impact of crossflow velocity on the hydrodynamics and specific energy consumption ($D = 5.2$ mm, $L = 3$ m, DS = 10 g/L, $T = 15$ °C)

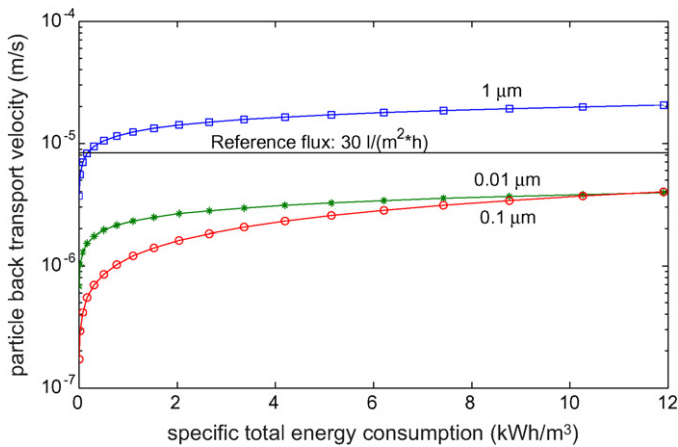| Crossflow velocity (m/s)	Re	Headloss ($\times 10^5$ Pa (bar))	$\hat{E}_c$ (kWh/m³)	$\hat{E}_f$ (at 30 L/m² h) (kWh/m³)	$\hat{E}_{tot}$ (kWh/m³)
0.23	466	0.010	0.004	0.004	0.008
0.50	1030	0.040	0.036	0.004	0.040
0.75	1540	0.082	0.108	0.004	0.112
1.00	2060	0.136	0.241	0.004	0.245
2.00	4111	0.456	1.610	0.004	1.614
3.00	6171	0.928	4.920	0.004	4.924
4.00	8222	1.533	10.832	0.004	10.836

Fig. 2. The influence of specific total energy consumption (by varying crossflow velocities) on the particle backtransport velocity for three particle radii (□, 0.01 μm; *, 0.1 μm; ○, 1 μm) ($D = 5.2$ mm, $L = 3$ m, DS = 10 g/L, $T = 15\,°C$).

Fig. 3. The relative sensitivity (RS) of particle backtransport and specific total energy consumption with respect to crossflow velocities ($a = 0.1$ μm, DS = 10 g/L, $D = 5.2$ mm, $L = 3$ m, $T = 15\,°C$).

0.5 m/s. The colloidal particles (<0.45 μm) in a MBR, e.g., SMP, are mostly produced due to microbial activity during the biomass growth and decay phases [30,31]. The operation of the MBR biology should therefore aim at reducing the SMP production or improve their degradation.

Fig. 2 illustrates the particle backtransport velocities for three particle radii (0.01, 0.1 and 1 μm) as a function of the specific total energy consumption as the crossflow velocity is varied. A specific total energy consumption higher than 2 kWh/m^3 (corresponding CF is 2.2 m/s) hardly improves the particle backtransport velocity, suggesting that for submicron particles, increasing the crossflow velocity would have less gain (controlling particle deposition) above a certain value. This phenomenon may be explained by the fact that the backtransport mechanism of small colloidal particles is mainly controlled by Brownian diffusion, and is therefore not sensitive to the shear rate (only a power of 0.33 in Eq. (13)).

5.2. Sensitivity analysis

The influence of design/operational variables on the headloss of the recirculating flow (h_f), the specific total energy consumption ($\hat{E}_{tot}$) and the particle backtransport velocity (J_{tot}) is quantified using either relative sensitivity (RS) or absolute sensitivity (AS) in Table 4. A positive sensitivity indicates a positive correlation, and larger RS values indicate higher influence, and vice vers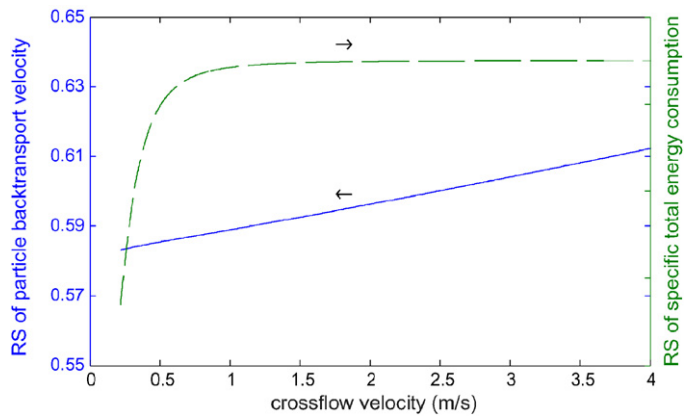a. Comparing the magnitudes of RS, the crossflow velocity and the dry solid contents have the most significant impact on the particle backtransport velocity. In the case that the sign of $\hat{E}_{tot}$ and J_{tot} are opposite, e.g., for the DS case, one can minimize DS to achieve a reduced energy consumption and improved particle backtransport. However, in the cases that $\hat{E}_{tot}$ and J_{tot} have the same sign, e.g., increasing the CF, the particle backtransport is improved but at the expense of more energy. Consequently, an optimization is needed. Detailed optimizations are given in Sections 5.4 and 5.5.

It should be noted that TMP distribution along the membrane tube is influenced by the friction headloss, which is strongly impacted by the crossflow velocity (RS = 1.75), membrane tube diameter (RS = −1.24) and tube length (RS = 1). In addition to the high crossflow velocity, small tube diameters and long lengths can also result in significant headloss and heterogeneous distribution of TMP. This phenomenon is not considered in this sensitivity analysis and should be avoided in the design of membrane modules.

The RS of $\hat{E}_{tot}$ and J_{tot} with respect to the crossflow velocity is plotted in Fig. 3. The RS of J_{tot} (0.58–0.61) is much lower than the one of $\hat{E}_{tot}$ (1.4–2.8), which suggests that the relative improvement in particle backtransport is less than the relative increase in energy consumption. Fortunately, the RS of J_{tot} remains high even at high crossflow velocities. Thus, increasing the crossflow velocity is still effective in fouling control throughout the crossflow velocity range (0.2–4 m/s). In order to adapt to the variation of fluxes (e.g., the diurnal flow rate profile

Table 4
The sensitivity of headloss, specific energy consumption and backtransport velocity with respect to operational variables (at conditions in Tables 1 and 2)

MBR variable	Headloss (h_f)	Specific energy consumption ($\hat{E}_{tot}$)	Backtransport velocity (J_{tot})	Other
Particle radius (a)	Null	Null	0.079	
Crossflow velocity (U)	1.75	2.69	0.59	
Membrane tube diameter (D)	−1.24	−0.24	−0.14	+Membrane manufacture cost
Membrane length (L)	1	0	−0.32	−Membrane manufacture cost
Dry solid contents (DS)	0.23	0.23	−0.85	−Construction cost of bioreactor
Temperature (T)	−92 Pa	−0.0016 kWh	7.54×10^{-8} m/s	−Particle breaking up

All sensitivities are RS except for the temperature, which is AS.

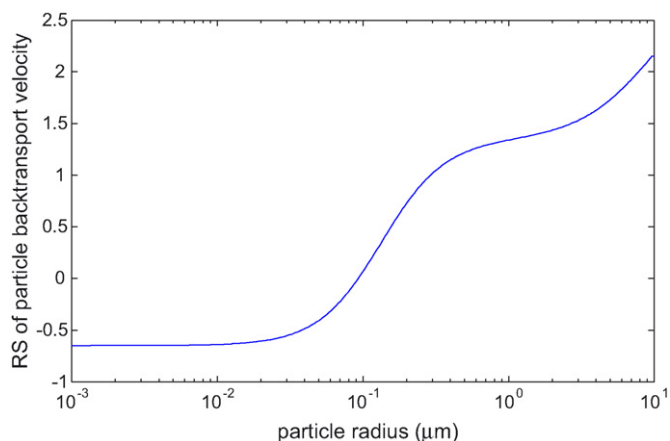Fig. 4. The relative sensitivity (RS) of the particle backtransport velocity with respect to particle radii (U = 1 m/s, DS = 10 g/L, D = 5.2 mm, L = 3 m, T = 15 °C).

of typical municipal WWTPs), side-stream MBRs can/should incorporate a certain control of the crossflow velocity, e.g., for long-term operation, a low CF may be applied under low flux conditions to save energy, and for short periods of operation, a high CF may be applied to handle high fluxes (peak flows). However, in submerged MBRs, the efficiency of coarse bubble aeration on fouling control generally decreases with increasing aeration density and eventually may saturate [32]. The flexibility of CF control to handle membrane fouling under highly dynamic flux conditions is an advantage of side-stream MBRs compared to the submerged ones.

Finally, the sensitivity of the particle backtransport velocity on various particle radii is plotted in Fig. 4. The sensitivity of the particle backtransport with respect to bigger particles is much higher than the submicron particles, and the most insensitive sizes have radii of approximately 0.1 µm. The colloids below 0.1 µm have negative sensitivities, which is due to the dominance of Brownian diffusion.

5.3. Particle size distribution in a lab-scale MBR

The particle size distribution (PSD) of the lab-scale MBR sludge is presented in Fig. 5. The MBR sludge showed a main peak at around 40 µm (flocs) and a second peak in the range of 0.1–1 µm (colloids). The colloidal peak may be bacteria cell or
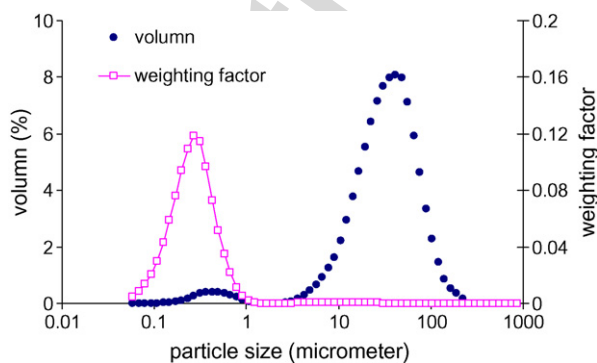

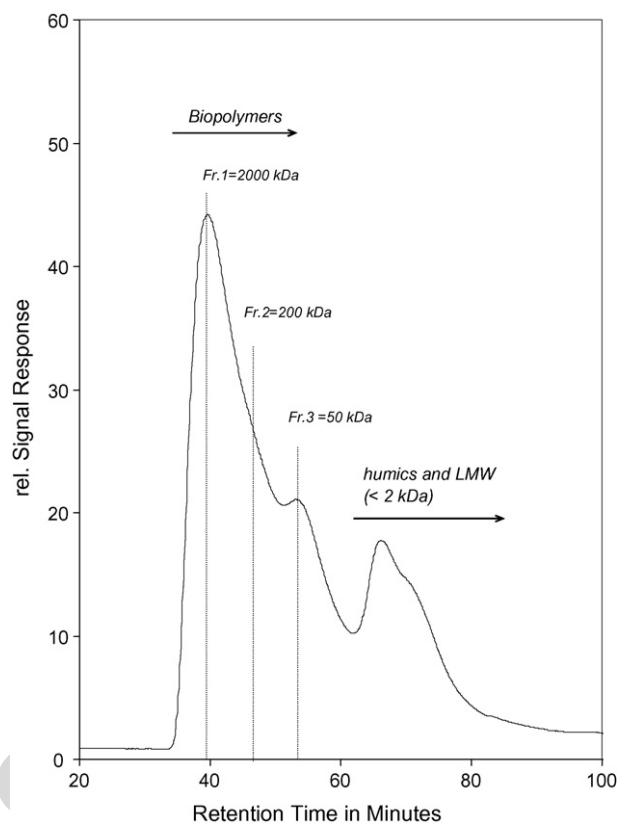Fig. 5. Particle size distribution and particle size weighting factor of lab-scale MBR sludge.

Fig. 6. LC-OCD chromatogram of SMP (PSD of submicron particles) of lab-scale MBR sludge water.

cell fragments. Many MBR studies showed a similar bimodal PSD. Sperandio et al. and Masse et al. reported the second peak was in the 1–10 µm range [33,34] and Wisniewski et al. reported the second peak at around 1–2 µm [29]. However, it should be noted that the submicron particle measurement using Malvern may not be reliable due to the uncertainty in the optical properties (i.e., the refractive index) of particles in biological systems.

To confirm the PSD of submicron particles, a LC-OCD was used to measure the sludge water (Fig. 6). The size exclusion chromatography (SEC) separates particles according to their sizes. The results suggested most submicron organic particles were biopolymers. The DOC of the 3 biopolymer fractions, i.e., 2000 kDa (i.e., approximately 0.2 µm), 200 kDa (0.02 µm) and 50 kDa (0.005 µm) were 21.0, 3.18 and 4.65 mgDOC/L, respectively. The very small colloids, e.g., humics, low molecular weight acids and neutrals (<2 kDa) amount to 12.5 mgDOC/L. The sum of the submicron particles (<0.45 µm) measured using Malvern was approximately 187 mg/L. This value was in the same magnitude with the estimation using the TOC of sludge water, i.e., 48.2 mgTOC/L, if one assumes the carbon content of particles is 44% (polysaccharide).

5.4. Theoretical optimization of MBR operation

Particle backtransport velocity and energy consumption should be optimized to maximize the energy efficiency in a side-stream MBR. An objective function (OBJ), Eq. (18), is constructed to maximize the gain of particle backtransport velocity

(J_{tot}) for the specific expense of energy ($\hat{E}_{tot}$) under various operational conditions (U, DS, D, L and T). If the PSD of a MBR sludge (based on volume) is known, a weighting factor (w_i Eq. (19)) can be included into the OBJ. The w_i is assumed inversely proportional to the square of the particle size based on the cake filtration mechanism (Kozeny-Carman relationship) [35].

$$OBJ = \sum_{w_i=a_{min}}^{a_{max}} \frac{w_i * J_{tot,i}}{\hat{E}_{tot}} \quad (18)$$

where i is a particle size class in a specific size range; a_{min} and a_{max} are the smallest and largest particle class radii; and $J_{tot,i}$ is the backtransport velocity of class i particles.

$$w_i = \frac{p_i}{a_i^2} \quad (19)$$

where p_i is the percentage of a specific particle class i; a_i is its particle class size.

Using the PSD of the lab-scale MBR sludge, the weighting factor (w_i) is plotted as a function of particle diameter in Fig. 5. It is interesting to see that high weighting factors lie in the range of the submicron particles, although the peak of the PSD is at around 40 μm. This suggests that the submicron particles have a high filter cake formation potential even when their quantity (in terms of volume) is small. It should be noted that the above calculation of w_i does not consider hydrodynamic effects, as they have been included in $J_{tot,i}$.

A nonlinear optimization with five operational variable constraints (U, DS, D, L and T) was formulated to maximize the objective function Eq. (18). A nonlinear programming (NLP) problem was solved using GAMS software [36]. The operational variables were constrained in the practical MBR operational range, i.e., $U = 0.5$–4 m/s, DS = 5–30 g/L, $D = 2$–10 mm, $L = 1$–5 m, and $T = 5$–30 °C. The particle size is an independent variable, thus a series of optimization steps were performed for each particle size (0.01–100 μm). Consequently no weighting factors are used in this theoretical optimization. The optimization results show that the optimal operation conditions of five variables all coincide with the boundary conditions (i.e., $U = 0.5$ m/s, DS = 5 g/L, $D = 2$ mm, $L = 1$ m and $T = 30$ °C) in spite of the particle sizes.

Due to the significance of crossflow velocity, an optimization of CF is presented in Fig. 7 using the PSD and weighting factors obtained in the lab-scale MBR under typical MBR operational conditions (DS = 10 g/L, $D = 5.2$ mm, $L = 3$ m, $T = 15$ °C). The result shows that operating the MBR under low crossflow velocities and allowing a certain degree of fouling can maximize the OBJ, which is evaluated as optimal. Operating under high crossflow velocities to achieve a high flux is not economical in long-term operation due to the high energy consumption.

5.5. Practical optimization of crossflow velocity in a lab-scale MBR

The influence of CF on particle deposition and membrane fouling was investigated in a lab-scale MBR system ($U = 0.5$–1.5 m/s), and the results were compared with the non-
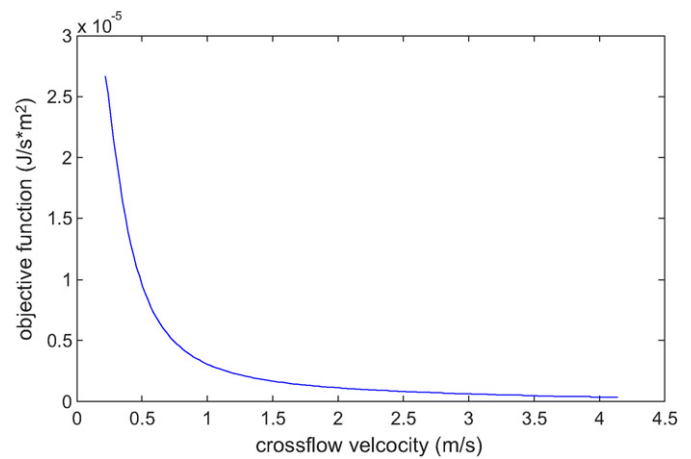

Fig. 7. Optimizing of crossflow velocity using the PSD of a lab-scale MBR sludge (DS = 10 g/L, $D = 5.2$ mm, $L = 3$ m, $T = 15$ °C).

stirred cell batch filtration system. In order to compare filtration performances, a new parameter is defined, i.e., the normalized fouling rate (NFR), as the increase in filtration resistance (m^{-1}) when one mgCOD (or DOC) is delivered to one m^2 membrane surface area. The NFR only counts the delivered COD or DOC in the sludge water phase (<0.45 μm). However, the particulate phase (>0.45 μm) is not considered as "delivered COD", since they have low tendency to deposit and low correlation with MBR fouling [5–8]. Therefore, the difference in NFR in the batch and online filtration should be mainly due to the hydrodynamic conditions, i.e., CF in the experiment.

The influence of CF is presented in Table 5. There are a few interesting points: (1) generally, increasing CF reduced the NFR, which was more pronounced at high flux and high fouling rate conditions (e.g., 50 L/(m^2 h)). However, a too high CF was not always beneficial with respect to fouling control (e.g., the NFR doubled as the CF increased from 1 to 1.5 m/s at 40 L/(m^2 h)). This strange behaviour may be due to the heterogeneous distribution of TMP. It was estimated using the above developed model that the TMP at the membrane inlet was 4.5–9.2 kPa higher than the outlet, as CF was increased from 1 to 1.5 m/s. The higher TMP in the membrane inlet created a higher flux, which probably exceeded the critical flux [37]. (2) At 40 L/(m^2 h), doubling the CF from 0.5 to 1 m/s reduced the NFR by a factor of 20, although the backtransport velocity of 0.2 μm particles (the main fraction of SMP) was merely doubled. This suggests that a critical CF value probably exists, below which, the fouling is significantly intensified, and above which, fouling is not further reduced. In this lab-scale MBR, this critical CF was between 0.75 and 1 m/s at 40 L/(m^2 h), which may be connected to the change from laminar to turbulent flow (Re increased from 1030 to 2060 as CF increased from 0.75 to 1 m/s). (3) The permeation velocities at 40 and 50 L/(m^2 h), i.e., 1.1 and 1.4 × 10^{-5} m/s, respectively, were actually much higher than the backtransport velocities, predicted by the sum effects of the Brownian diffusion, shear-induced diffusion and inertial lift. It appears that either other hydrodynamic mechanisms controlled particle deposition, or that other physical/chemical factors played a role, e.g., the electrostatic repulsion between colloidal particles.

Table 5
The impact of hydrodynamic condition (dead-end vs. various CF velocities) on MBR fouling

Crossflow velocity (m/s)	Re	Specific resistance to filtration (dR/dCOD_delivered, m/mgCOD)		Backtransport velocity of 0.2 μm particles (m/s)
		40 L/(m^2 h)	50 L/(m^2 h)	
0 (dead-end batch filtration)	0	3.81×10^9	3.81×10^9	$<9.17 \times 10^{-7}$
0.5	1030	20.3×10^8	n.a.	4.92×10^{-7}
0.75	1540	5.90×10^8	n.a.	6.91×10^{-7}
1	2060	1.03×10^8	15.1×10^8	9.06×10^{-7}
1.5	3081	2.23×10^8	7.15×10^8	13.8×10^{-7}

Dead-end and online crossflow MBR filtration were compared using the NFR and the theoretical calculation of particle backtransport velocity (Table 5). The NFR at $U = 0.5$ m/s was just 53% of the NFR in dead-end filtration, i.e., the 0.5 m/s CF only reduced 47% of the membrane fouling. This suggests that the CF was too low to effectively control the deposition of colloidal particles in the sludge water phase. In the dead-end batch filtration, an ultimate filtration flux was stabilized at 3.30 L/(m^2 h) in 10 h. According to the classical concentration polarization model [35,38], at a critical cake formation condition, the particle backtransport velocity can be assumed to equal this ultimate permeation flux, i.e., 9.17×10^{-7} m/s. Consequently, the actual particle backtransport velocity in the batch filtration should be lower than this value, since a cake was built up. However, it should be noted that the estimation of particle backtransport presented here is rather rough. A more précised model considering other factors should be considered in the future study, e.g., combined effects of different particle sizes.

6. Conclusions

An integrated hydrodynamic model was developed by combining particle backtransport and energy consumption in tubular MBR systems. The model is able to predict the effects of feed sludge particle size (a), dry solid contents (DS), crossflow velocity (U), membrane tube dimension (D and L) and temperature (T) on the particle transportation and energy consumption. The theoretical simulation focused on submicron particles and the crossflow velocity in a full-scale tubular membrane module. The results showed that the submicron particles had a high likelihood to deposit, and the worst fouling region was with particle radii around 0.1 μm and crossflow (CF) velocity below 0.5 m/s. Simply increasing CF did not completely prevent colloidal particle deposition.

The sensitivity analysis concluded the impact of CF is significant, while other operational variables (DS, D, L and T) were generally less influential. However, care should be taken in designing the membrane tube diameter and length. Membrane tubes with too small diameters and long lengths can result in a heterogeneous TMP distribution and therefore a higher flux and membrane fouling in the membrane inlet than the outlet. Introducing air into the feed side (air-lift) can partially counterbalance this problem in vertical membrane module systems.

The particle size distribution showed that a lab-scale MBR sludge showed a second peak in the colloidal region (0.1–1 μm)

in addition to a main peak at 40 μm, which was confirmed by liquid chromatography–organic carbon detection (LC-OCD) measurement of sludge water with a high biopolymer fraction at 2000 kDa. In the optimization, the submicron particles received high weighting factors (high filter cake formation potential) although their quantity was small. The theoretical optimization considering the typical PSD suggests that cost-effective operation of an MBR is at the lowest possible crossflow velocity. However, the practical optimization in a lab-scale MBR concludes that the crossflow velocity should neither be too low such that dead-end conditions are approached, nor too high to result in heterogeneous TMP distribution and increased energy consumption. A critical CF value probably exists, below which, the fouling is significantly intensified, and above which, fouling is not further reduced. In this lab-scale MBR, this critical CF was between 0.75 and 1 m/s at 40 L/(m^2 h).

7. Recommendations

The models presented here assumed ideal particles and no particle–particle interactions. However, the flocs and submicron particles are not perfect spheres, and some may even be porous. They may deform, aggregate and break up in both the bulk and boundary layer and inside the filter cake. The contributions of all these effects to the hydrodynamic models presented in this manuscript are unknown and will need to be addressed in future model structures and analyses.

A control algorithm for the crossflow velocity can be developed based on this study, e.g., for long-term low flux operation, low CF can be used to save energy and for short-term high flux (fouling) conditions, high CF can be employed to handle flux peaks. Finally, this study indicated the difficulty in controlling the deposition of submicron particles using only a hydrodynamic approach, therefore operation of MBR biology should aim at reducing the SMP production and improve SMP degradation, to reduce the fraction of particles in the colloidal range.

Nomenclature

a	particle radius (m)
A	total membrane surface area (m^2)
D	membrane tube diameter (m)
D_B	Brownian diffusion coefficient (m^2/s)
DS	sludge dry solid contents (g/L)
E_c, E_f	energy consumption due to crossflow and filtration (W)
$\hat{E}_c, \hat{E}_f$	specific energy consumption due to crossflow and filtration producing unit permeate (J/m^3, kWh/m^3)
$\hat{E}_{tot}$	total specific energy consumption (J/m^3, kWh/m^3)
f	Darcy friction factor
h_f	headloss of feed sludge passing through membrane tube (m water column ($\times 10^5$ Pa (bar))
J_f, J_{BW}	filtration flux and backwashing flux (L/(m^2 h), m/s)
J_B, J_I, J_s	backtransport velocity of Brownian diffusion, inertial lift and shear-induced diffusion (L/(m^2 h), m/s)
J_{tot}	total backtransport velocity (L/(m^2 h), m/s)
k	Boltzmann constant (1.38×10^{-23} kg m^2/s^2)
L	membrane tube length (m)
p_i	percentage of a specific particle class
$\Delta P_{BW}, \Delta P_f$	pressure difference during backwashing and filtration ($\times 10^5$ Pa, bar)
Q	volumetric flow rate (m^3/s)
t_{BW}, t_f	duration of one backwashing and filtration cycle (s)
t_{tot}	total cycle time (filtration + backwashing) (s)
T, T_0	absolute temperature and standard absolute temperature (293.15 K) (K)
U	crossflow velocity (m/s)
w_i	weighting factor for class i
$x, \Delta x$	input parameters/variables and their variation
$y, \Delta y$	output variables and their variation

Greek letters

γ_w	shear rate at the surface of the membrane (s^{-1})
η_f, η_{f0}	dynamic viscosity of feed flow and at standard temperature (Pa s)
Φ_b, Φ_w	particle volume fraction in the bulk and wall
$\rho_f, \rho_p, \rho_{DS}$	density of activated sludge, permeate and dry solid (kg/m^3)
τ_w	wall shear stress (Pa)

References

[1] S. Judd, The MBR Book: Principles and Applications of Membrane Bioreactors, Elsevier, Boston, MA, 2006.

[2] C. Wisniewski, A. Grasmick, Floc size distribution in a membrane bioreactor and consequences for membrane fouling, Colloids Surf. A-Physicochem. Eng. Aspects 138 (1998) 403.

[3] L. Defrance, M.Y. Jaffrin, B. Gupta, P. Paullier, V. Geaugey, Contribution of various constituents of activated sludge to membrane bioreactor fouling, Bioresour. Technol. 73 (2000) 105.

[4] E. Bouhabila, R. Ben Aim, H. Buisson, Fouling characterisation in membrane bioreactors, Sep. Purif. Technol. 22-3 (2001) 123.

[5] M.E.H. Rojas, R. Van Kaam, S. Schetrite, C. Albasi, Role and variations of supernatant compounds in submerged membrane bioreactor fouling, Desalination 179 (2005) 95.

[6] B. Lesjean, S. Rosenberger, C. Laabs, M. Jekel, R. Gnirss, G. Amy, Correlation between membrane fouling and soluble/colloidal organic substances in membrane bioreactors for municipal wastewater treatment, Water Sci. Technol. 51 (2005) 1.

[7] S. Rosenberger, C. Laabs, B. Lesjean, R. Gnirss, G. Amy, M. Jekel, J.C. Schrotter, Impact of colloidal and soluble organic material on membrane performance in membrane bioreactors for municipal wastewater treatment, Water Res. 40 (2006) 710.

[8] S. Rosenberger, H. Evenblij, S.T. te Poele, T. Wintgens, C. Laabs, The importance of liquid phase analyses to understand fouling in membrane assisted activated sludge processes—six case studies of different European research groups, J. Membr. Sci. 263 (2005) 113.

[9] S.T. te Poele, J.H. Roorda, J.H.J.M. van der Graaf, Influence of the size of membrane foulants on the filterability of WWTP-effluent, Water Sci. Technol. 50 (2004) 111.

[10] G. Belfort, R.H. Davis, A.L. Zydney, The behavior of suspensions and macromolecular solutions in cross-flow microfiltration, J. Membr. Sci. 96 (1994) 1.

[11] E. Tardieu, A. Grasmick, V. Geaugey, J. Manem, Hydrodynamic control of bioparticle deposition in a MBR applied to wastewater treatment, J. Membr. Sci. 147 (1998) 1.

[12] E. Tardieu, A. Grasmick, V. Geaugey, J. Manem, Influence of hydrodynamics on fouling velocity in a recirculated MBR for wastewater treatment, J. Membr. Sci. 156 (1999) 131.

[13] T. Jiang, M.D. Kennedy, W.G.J. van der Meer, P.A. Vanrolleghem, J.C. Schippers, The role of blocking and cake filtration in MBR fouling, Desalination 157 (2003) 335.

[14] M. Gander, B. Jefferson, S. Judd, Aerobic MBRs for domestic wastewater treatment: a review with cost considerations, Sep. Purif. Technol. 18 (2000) 119.

[15] Z.F. Cui, S.R. Bellara, P. Homewood, Airlift crossflow membrane filtration—a feasibility study with dextran ultrafiltration, J. Membr. Sci. 128 (1997) 83.

[16] S.A. Huber, F.H. Frimmel, Flow-injection analysis of organic and inorganic carbon in the low-ppb range, Anal. Chem. 63 (1991) 2122.

[17] F.M. White, Fluid Mechanics, McGraw-Hill, Inc., New York, 1986.

[18] G. Tchobanoglous, F.L. Burton, H.D. Stensel, Wastewater Engineering: Treatment and Reuse, McGraw-Hill, Boston, 2003.

[19] N. Tixier, G. Guibaud, M. Baudu, Determination of some rheological parameters for the characterization of activated sludge, Bioresour. Technol. 90 (2003) 215.

[20] R.H. Davis, Modeling of fouling of cross-flow microfiltration membranes, Sep. Purif. Methods 21 (1992) 75.

[21] W.R. Bowen, A.O. Sharif, Hydrodynamic and colloidal interactions effects on the rejection of a particle larger than a pore in microfiltration and ultrafiltration membranes, Chem. Eng. Sci. 53 (1998) 879.

[22] A.L. Zydney, C.K. Colton, A concentration polarization model for the filtrate flux in cross-flow microfiltration of particulate suspensions, Chem. Eng. Commun. 47 (1986) 1.

[23] R.H. Davis, J.D. Sherwood, A similarity solution for steady-state cross-flow microfiltration, Chem. Eng. Sci. 45 (1990) 3203.

[24] G. Green, G. Belfort, Fouling of ultrafiltration membranes—Lateral migration and the particle trajectory model, Desalination 35 (1980) 129.

[25] D.A. Drew, J.A. Schonberg, G. Belfort, Lateral inertial migration of a small sphere in fast laminar-flow through a membrane duct, Chem. Eng. Sci. 46 (1991) 3219.

[26] G. Boeije, R. Corstanje, A. Rottiers, D. Schowanek, Adaptation of the CAS test system and synthetic sewage for biological nutrient removal—Part I: development of a new synthetic sewage, Chemosphere 38 (1999) 699.

[27] N. Engelhardt, W. Lindner, Experiences with the world's largest municipal waste water treatment plant using membrane technology, Water Practice Technol. 1 (2006).

[28] B. Zhang, K. Yamamoto, S. Ohgaki, N. Kamiko, Floc size distribution and bacterial activities in membrane separation activated sludge processes for small-scale wastewater treatment/reclamation, Water Sci. Technol. 35 (1997) 37.

[29] C. Wisniewski, A. Grasmick, A.L. Cruz, Critical particle size in membrane bioreactors—case of a denitrifying bacterial suspension, J. Membr. Sci. 178 (2000) 141.

[30] E. Namkung, B.E. Rittmann, Soluble microbial products (SMP) formation kinetics by biofilms, Water Res. 20 (1986) 795.

[31] B.E. Rittmann, W. Bae, E. Namkung, C.J. Lu, A critical-evaluation of microbial product formation in biological processes, Water Sci. Technol. 19 (1987) 517.

[32] J.A. Howell, H.C. Chua, T.C. Arnot, In situ manipulation of critical flux in a submerged membrane bioreactor using variable aeration rates, and effects of membrane history, J. Membr. Sci. 242 (2004) 13.

[33] M. Sperandio, A. Masse, M.C. Espinosa-Bouchot, C. Cabassud, Characterization of sludge structure and activity in submerged membrane bioreactor, Water Sci. Technol. 52 (2005) 401.

[34] A. Masse, M. Sperandio, C. Cabassud, Comparison of sludge characteristics and performance of a submerged membrane bioreactor and an activated sludge process at high solids retention time, Water Res. 40 (2006) 2405.

[35] M. Mulder, Basic Principles of Membrane Technology, Kluwer Academic, Dordrecht; Boston, 1996.

[36] A. Brooke, D. Kendrick, A. Meeraus, R. Raman, GAMS–A User's Guide, GAMS Development Corporation, Washington, USA, 1998.

[37] A.G. Fane, S. Chang, E. Chardon, Submerged hollow fibre membrane module—design options and operational considerations, Desalination 146 (2002) 231.

[38] V. Chen, A.G. Fane, S. Madaeni, I.G. Wenten, Particle deposition during membrane filtration of colloids: transition between concentration polarization and cake formation, J. Membr. Sci. 125 (1997) 109.